Monoblock Antenna-Loaded Filter Pair: Synthesis, Model Extraction, and EM Design

Xiao Tan, Yuliang Chen, *Member, IEEE*, and Ke-Li Wu, *Fellow, IEEE*

***Abstract*— This article proposes a monoblock module incorporating a dual-polarized patch antenna and two symmetrical channel filters, forming an integrated antenna-loaded filter (ALF) pair, for the first time. The module offers high-frequency selectivity, stable gain, compact size, and low insertion loss. To address design challenges, a generic synthesis and electromagnetic (EM) design framework is also proposed. In this framework, the antenna is treated as a frequency-variant complex load to the filter, and the filter network is synthesized by fully considering the antenna characteristics. This approach allows for higher design freedom. To preserve the intrinsic radiation characteristics and enhance the matching bandwidth, three practical strategies are innovated: introducing a buffer resonator to the antenna, creating an air cavity under the patch antenna, and feeding the patch antenna with a dielectric waveguide. The concept of a virtual-insignificant-port (VIP) model is introduced for extracting the overall circuit model of the ALF for deterministic EM design. The proposed framework is demonstrated with step-by-step details, showcasing its flexibility, convenience, and versatility for ALF modules. The validity of the monoblock ALF module is affirmed by a ceramic-based prototype, whose experimental results exhibit excellent impedance matching, frequency selectivity, and radiation properties.**

***Index Terms*— Complex impedance, dielectric resonators, filter synthesis, filtering antennas, impedance matching, patch antennas.**

I. Introduction

THE compactness, low insertion loss, and simplicity of a microwave passive front-end assembly are three everlasting demands for communication systems, especially in base stations for wireless communications. With the massive multi-input multi-output (M-MIMO) antenna technology becoming the most popular spatial multiplexing scheme, the efficiency and compactness of the affiliated antenna elements and their adjoint bandpass filters, the two most critical passive components for the front end, are the two most crucial aspects to be addressed. Due to the strict rejection specification for bandpass filters and the incompatibility of the form factors for antennas and filters, the antenna elements and filters in a traditional RF front end are individually designed to match a 50-Ω load and then assembled through transmission lines (TLs). Such an assembly scheme inevitably leads to a larger size, additional insertion loss, and significant performance variation, especially when the number of transceiver channels is high.

The concept of integrating an antenna with a bandpass filter can be traced back to 1998 [1]. It proposed and demonstrated a multifunctional antenna/filter device that integrates a uniplanar slotline dipole with a Chebyshev bandpass filter. The concept was also demonstrated by a "radiant filter" [2], where a two-pole Chebyshev filtering response was realized by two vertically stacked high-Q parallelepipedal cavities with a radiating opening on the top surface.

In recent years, there has been a growing interest in consolidating a filtering function into an antenna, known as a "filtering antenna," aiming at high frequency selectivity, stable gain, compact size, and low insertion loss simultaneously. There are mainly three types of filtering antenna schemes in the literature. The first type is the cascading scheme, in which an antenna radiator is directly connected to a filter [3], [4], [5], [6], [7], [8], [9], [10] while serving as the last resonator of the filter. This scheme is straightforward and usually employs a conventional antenna and filter form factor. The antenna radiation resistance is adjusted to match the required external Q of the conventionally synthesized filter. In other words, the matching bandwidth of the antenna must be broader than that of the bandpass filter [3] and the radiating properties of the antenna may need to be sacrificed to accommodate the synthesized filter as if the filter were terminated by real loads. In many applications, a wideband antenna may not always be available, especially for an antenna made of a dielectric substrate with high permittivity.

The second type is the emerging scheme, in which a simple resonant structure is merged with the antenna feeding structure [11], [12], [13], [14], [15], [16], creating a certain degree of frequency selectivity. However, the resonant structures used are usually microstrip, which typically has low unloaded Q. The third type is the null-generating scheme that utilizes the parasitic resonance of the antenna or its associated feeding structure. Commonly used parasitic structures include open stubs, parasitic patches, shorting pins, slots on the radiator, and defected ground structures [17], [18], [19], [20], [21]. The generated radiation nulls usually appear far from the passband, which greatly limits the filtering ability. Additionally, the design is also highly specific to the antenna configuration.

Manuscript received 8 November 2023; revised 31 January 2024 and 5 March 2024; accepted 21 March 2024. This work was supported by the Postgraduate Scholarship of The Chinese University of Hong Kong. *(Corresponding author: Ke-Li Wu.)*

The authors are with the Department of Electronic Engineering, The Chinese University of Hong Kong, Hong Kong (e-mail: xtan@link.cuhk.edu.hk; ylchen@link.cuhk.edu.hk; klwu@ee.cuhk.edu.hk).

Color versions of one or more figures in this article are available at https://doi.org/10.1109/TMTT.2024.3381791.

Digital Object Identifier 10.1109/TMTT.2024.3381791

The works mentioned above are primarily antenna-centric, lacking either adequate control over the rejection rate or an efficient electromagnetic (EM) tuning technique for high filtering performance. In practice, many applications require a filter-centric approach, aiming to design a high-performance filtering response that fulfills not only the matching condition but also the transmission characteristics for a given transmission zero (TZ) arrangement. Such an integrated multifunctional module is referred to as an antenna-loaded filter (ALF) in this context, where the antenna and filter become inseparable, not only in physical form but also from synthesis to EM design.

In this work, a generic framework for the synthesis and deterministic EM design of an ALF module is proposed. The filter circuit model is synthesized with full consideration of the given antenna characteristics instead of sacrificing the intrinsic radiation properties of the antenna. The synthesized circuit model is then used as the EM design objective of the integrated ALF module. The framework is demonstrated by a prototyped monoblock dielectric resonator (MDR) filter pair loaded with a dual-polarized patch antenna.

The MDR ALF module is conceptually proposed and physically demonstrated in this work for the first time. The bandpass filter pair is realized using MDR technology with a high dielectric constant (ceramic). Compared to traditional microstrip or metallic cavity filters, MDR filters offer a compact size while maintaining a high unloaded Q, low insertion loss, and flexible TZ placement [22], [23], [24], [25]. To ensure compatibility with an MDR filter, a patch antenna on the same dielectric substrate and a novel feeding structure using a short dielectric waveguide are utilized, as briefly reported in [26]. Furthermore, the bandwidth of the ALF, made of a ceramic block with a high dielectric constant, is extended by introducing a buffer resonator and a partial air cavity in the antenna substrate. The monoblock dual-polarized patch ALF module incorporates two symmetrical 6-2 (six-pole with two TZs) channel filters operating in the 3.5–3.72 GHz band. The two bandpass filters and the dual-polarized patch antenna are integrated into a single ceramic monoblock.

With the optimal antenna radiation characteristic achieved, the bandpass filter circuit model is analytically synthesized by considering the antenna as a frequency-variant complex load at one port [27]. Unlike traditional design philosophy for filtering antennas, in which the antenna is adopted as the last resonator of the traditionally synthesized filter circuit model and the radiation resistance of the antenna has to be compromised to fit the required external Q of the filter circuit model, the general synthesis theory for an ALF treats the antenna and its auxiliary components as a whole as an external loading effect of the filter, rendering the highest degree of design freedom for the filter network and resulting in an optimal radiation, matching, and rejection performance of ALF. It will be demonstrated that the traditional filtering antenna synthesis fails in this example due to the narrowband antenna. To facilitate the deterministic EM design, a virtual-insignificant-port (VIP) model is proposed, which incorporates a weak-coupling port. This model enables an efficient filter-centric tuning process by extracting the overall circuit model of the ALF module. This work presents the following unique contributions:

1) The first monoblock dual-polarized patch ALF is conceptually proposed and physically demonstrated.
2) A generic filter-centric synthesis and deterministic EM design framework for an integrated ALF module is proposed for the first time, which is applicable for both wide and narrow-band antennas.
3) A novel concept of VIP is introduced for extracting the overall circuit model of an ALF, which is essential for deterministic EM design.
4) The novel dielectric waveguide feeding structure to the patch antenna is investigated and proved to be highly compatible with a monoblock ALF module.

In essence, this work introduces a systematic, efficient, and convenient framework for the synthesis and EM design of an integrated ALF module for the first time. The framework is highly versatile for developing filter-centric ALF modules. The details of the framework will be elaborated step by step through the design process of the monoblock ALF module. The ALF is synthesized, EM simulated, and measured with an excellent agreement, which is attributed to the systematic framework.

II. Configuration of the Monoblock ALF

The configuration of the proposed monoblock dielectric filter pair loaded with a dual-polarized patch antenna is depicted in Fig. 1. Each signal path for a polarization comprises an input/output (I/O) port (P1 or P2), a 6-2 coupled-resonator bandpass channel filter, a buffer resonator, and a shared-cavity patch antenna. Metallization is applied to all surfaces of the two monoblock bandpass filters and the metal patch antenna (in yellow). The metal patch is printed on the top surface of the dielectric substrate with a partial air cavity. The two linear polarizations are oriented at $\pm 45°$, making the module suitable for wireless base station applications. To enhance the matching bandwidth of the ALF, a buffer resonator is inserted between the sixth resonator of the filter and the antenna. The patch antenna is fed via a short dielectric waveguide extending from the chamfered side of the buffer resonator. An air cavity is partially excavated from the bottom of the antenna substrate to increase the antenna bandwidth. Since the antenna is settled in a complex and asymmetrical EM environment, which could cause an unwanted coupling between the two polarizations, the metal patch is chamfered at the upper and lower corners and offset by 0.2 mm toward the $-y$-direction from the center of the substrate to introduce an opposite coupling for cancellation so that the isolation between the two polarizations is enhanced.

The 6-2 bandpass filter comprises six quasi-TEM mode resonators, each of which is formed by a blind hole from the top with a radius of $r = 1.75$ mm. The required positive couplings are implemented by partitioning walls formed by a vertical channel cutting through the dielectric block. A cascaded quadruplet (CQ) coupling section, constructed by resonators 1-2-3-4, is used to generate two asymmetric TZs.

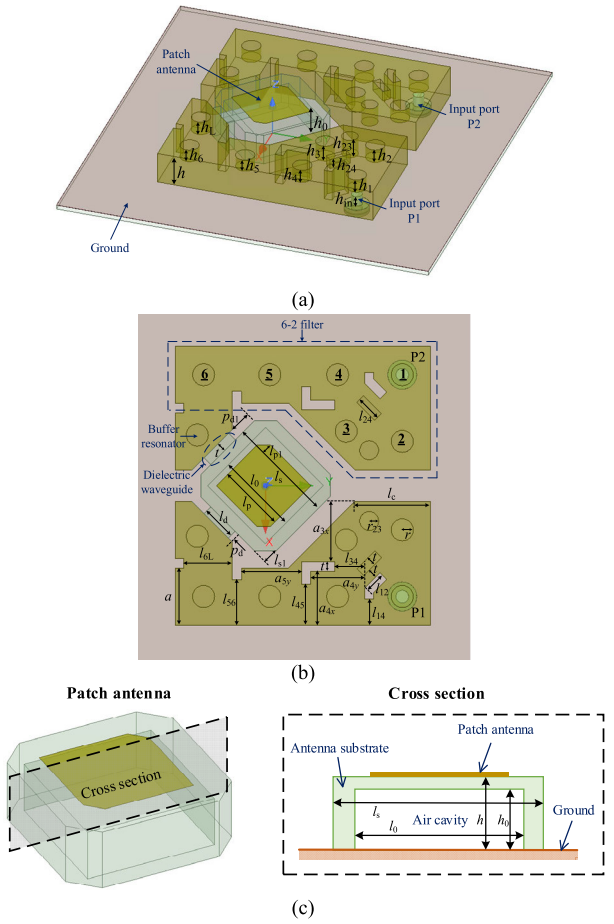

Fig. 1. Configuration of the dual-polarized MDR patch ALF with (a) perspective view, (b) top view, and (c) view on patch antenna only.

A blind metalized hole of radius $r_{23} = 1.5$ mm is positioned between resonators 2 and 3 to generate a negative coupling [22]. A blind diagonal ridge is strategically placed between resonators 2 and 4 to adjust the diagonal cross-coupling.

The dual-polarized patch antenna is situated in the inner core area of the monoblock module and is surrounded by the surface-metalized filter body, attempting to create a balanced EM environment. Resonator 3 is chamfered to provide sufficient clearance for the radiation edges of the patch antenna. The filter pair is symmetrically arranged with respect to the y-axis, whose origin is at the center of the antenna substrate. In the EM design model, the dielectric constant is set to 19.15 with a loss tangent of 5×10^{-5}. The conductivity of the metal surface is set to 3.5×10^7 S/m. The dimension for a regular resonator cavity is $9 \times 9 \times 6$ mm^3. Other specific dimensions are provided in Table I. Although the filter portion of the dual-polarized monoblock ALF module occupies a significant area relative to the antenna, the overall dimension is only $0.53 \times 0.49 \times 0.07\lambda_0^3$.

In the subsequent sections, the synthesis and EM design framework will be introduced in detail, including the model extraction of the antenna as a frequency-variant complex load, synthesis of the filter circuit model, and deterministic EM design procedure.

TABLE I
DIMENSIONS OF THE DUAL-POLARIZED MDR PATCH ALF IN EM MODEL

Parameter	a	a_{3x}	a_{4x}	a_{4y}	a_{5y}	t
Value (mm)	9	9.5	8.5	8.5	9.5	1.5
Parameter	h_{in}	h_1	h_2	h_{23}	h_{24}	h_3
Value (mm)	2	2.565	2.555	3.63	1.88	3.095
Parameter	h_4	h_5	h_6	h_L	h	h_0
Value (mm)	2.519	2.312	2.416	2.58	6	5
Parameter	l_{12}	l_{14}	l_{24}	l_{34}	l_{45}	l_{56}
Value (mm)	3.47	4.11	4	4.68	6.4	7.13
Parameter	l_{6L}	l_d	l_s	l_{s1}	l_p	l_{p1}
Value (mm)	7.65	5.45	17	2.5	10.55	1.5
Parameter	l_c	l_0	p_d	p_{d1}	r	r_{23}
Value (mm)	12	13	0.8	3.5	1.75	1.5

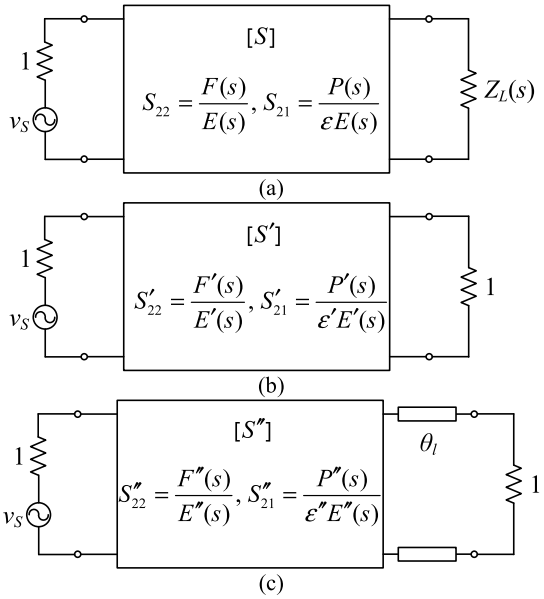

Fig. 2. (a) Desired filter network with complex load, (b) desired filter network with normalized impedance, and (c) realizable filter network + TL with normalized impedance.

III. FILTER SYNTHESIS WITH COMPLEX LOAD

In a general ALF module, the antenna can be considered as a frequency-variant complex load to the filter network. In other words, the synthesis of an ALF becomes a problem of synthesizing a filter network terminated by a complex load [27].

A. Basic Concept of Filter Synthesis With a Complex Load

In this section, the basic concept of directly synthesizing a bandpass filter with a complex load is reviewed here for convenience.

Consider the three filter networks shown in Fig. 2. The complex-loaded network with the *desired* S-parameters $[S]$ can be described by the system polynomial functions $[E(s), P(s), F(s)]$ as illustrated in Fig. 2(a), where s represents the complex frequency in the lowpass frequency domain. When the complex load is substituted with the unity reference impedance (normalized to the port impedance), as illustrated in Fig. 2(b), the response $[S']$ of the desired filter network becomes measurable. However, it may not be realizable using

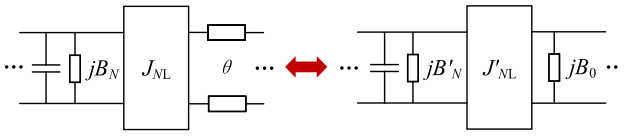

Fig. 3. Equivalent lowpass circuit transformation of the inserted TL at filter output.

a coupled-resonator network because its approximate characteristic functions described by polynomials $[E'(s), P'(s), F'(s)]$ are not necessarily monic. It can be shown that the response $[S']$ is equivalent to a realizable coupled-resonator network, whose response $[S'']$ can be described by polynomial functions $[E''(s), P''(s), F''(s)]$ as depicted in Fig. 2(c), cascaded with a TL of optimal length θ. According to the power wave renormalization theory [28], the relationship between $[S]$ and $[S']$ is well established, leading to the discovery of three mapping equations from (E, P, F) to (E', P', F') [27]

$$\text{Transference condition: } \frac{P'}{\varepsilon'} = 2\sqrt{\text{Re}\{Z_L\}}\frac{P}{\varepsilon} \tag{1a}$$

$$\text{Matchability condition: } F' = (1 + Z_L)F - \left(1 - Z_L^*\right)E \tag{1b}$$

$$\text{Conservation condition: } E' = \left(1 + Z_L^*\right)E - (1 - Z_L)F \tag{1c}$$

Although the above three equations stipulate the relationship between the filtering functions of the ideal desired response of a filter terminated by a *frequency variant* complex load and the measurable response of the same filter (with the matched load), it must be aware that the equations can only be satisfied *approximately* because the filtering function defined by (E', P', F') are polynomials of finite orders. Usually, higher priorities of the accuracy are given to (1a) and (1b) whereas (1c) is used for determining the optimal length θ_l (θ hereafter). Since (1) can only be satisfied approximately, achieving the ideally synthesized return loss as described by (E, P, F) cannot be warranted unless the loading effect is a constant complex [29].

In the context of the monoblock dielectric ALF, inserting a TL is not practical. Fortunately, the TL can be transformed into a frequency-invariant reactance (FIR) jB_0 [30], as illustrated in Fig. 3

$$B_0 = \tan\theta \tag{2a}$$

$$J'_{NL} = \frac{J_{NL}}{\cos\theta} \tag{2b}$$

$$B'_N = B_N + J_{NL}^2 \tan\theta \tag{2c}$$

The transformation implies that to optimally match the antenna while maintaining a strict rejection requirement, an additional FIR jB_0 needs to be introduced between the filter output and the antenna. There are two options to realize the FIR: 1) shifting the resonant frequency of the antenna by an amount of $-BW \cdot B_0/2$, where BW is the absolute bandwidth of the filter and 2) introducing a buffer resonator, represented by $(s + jB_L)$, prior to the antenna to absorb the FIR, as illustrated in Fig. 4. The former is a direct method but may degrade the radiation performance of the antenna from the

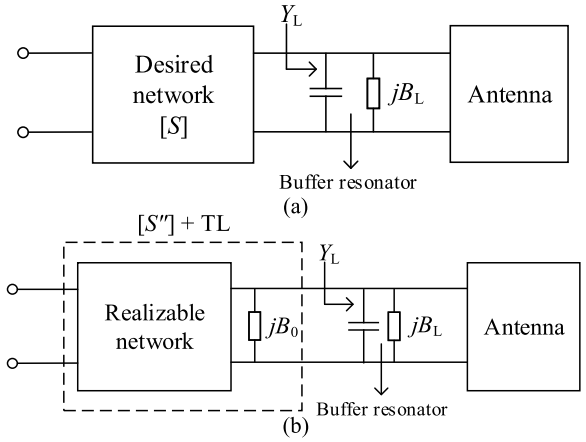

Fig. 4. Diagram of ALF with a buffer resonator between the filter network and the antenna (a) before synthesis and (b) after synthesis.

TABLE II
DIMENSIONS OF THE THREE-POLE MDR PATCH ALF

Parameter	h_{in}	h_6	h_L	l_{6L}	l_d	l_p	l_0	p_d
Value (mm)	2.3	2.41	2.52	7.8	5.65	10.5	13	0.4

optimal frequency with the highest radiation gain. The latter requires additional space but preserves the original radiation characteristic. When the antenna bandwidth is broad, the required FIR will be relatively small, and the frequency shift will not be a concern. However, when the antenna bandwidth is narrow, as in the case of a patch antenna on a substrate with a high dielectric constant and in complex conductive surroundings, the second option becomes a legitimate choice. In this scenario, the buffer resonator is introduced to enhance the matching bandwidth of the ALF module without altering the antenna's performance.

B. Circuit Model Extraction of Complex Load

To synthesize the complex-loaded filter network, the frequency-variant complex load needs to be extracted first with high fidelity. To accomplish this, two ad-hoc ports, one for each polarization signal path, are introduced at the adjacent resonators to the buffer resonators, as shown in Fig. 5. The adjacent resonator in the EM model, denoted as $(s + jB_1)$ in Fig. 6, is electrically isolated from the rest of the filter by a nearly full-width partitioning wall. Be noted that a roughly designed body of the monoblock ALF module is utilized as a dummy in the EM model to preserve the same EM scattering and radiation characteristics of the antenna, which contribute to the complex load significantly. The dual-polarized antenna is carefully designed to 1) maximize the gain bandwidth; 2) ensure that the highest gain occurs at the center frequency of the filter; and 3) achieve sufficiently high isolation between two ad-hoc ports. The dimensions that differ from those provided in Table I are listed in Table II.

Having understood the physical model for extraction of the complex load, the three-pole coupled-resonator network in the lowpass domain is shown in Fig. 6 to illustrate the process of extracting the circuit model for the complex load Y_L. In this network, the antenna is modeled as a single-pole

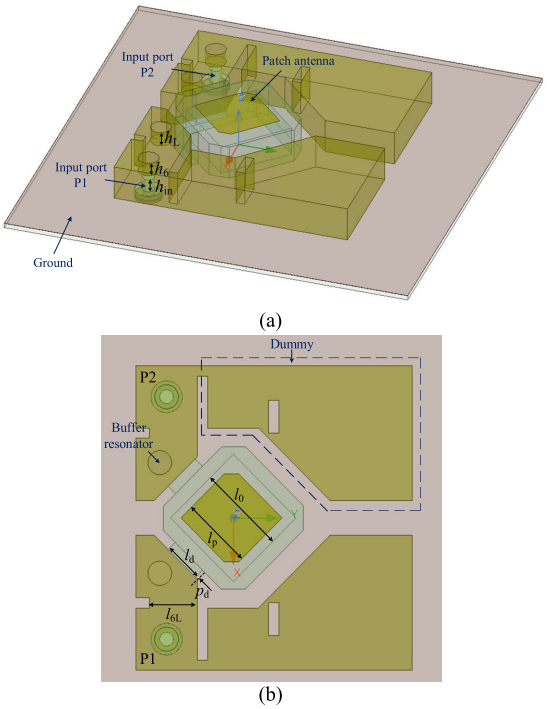

(a) (b)

Fig. 5. Configuration of the dual-polarized three-pole MDR patch ALF for extraction of the complex load, where P1 and P2 are the ad-hoc ports (a) perspective view and (b) top view.

lossy resonator ($s + jB_a$), where B_a is a complex number, whose unloaded Q is much lower than those of the resonators in the bandpass filters. The buffer resonator is represented by ($s + jB_L$), whose FIR jB_L will be adjusted by absorbing jB_0 once the filter synthesis with the antenna and buffer resonator as the complex load is completed. By introducing an ad-hoc port at the resonator ($s + jB_1$), the circuit description for Y_L, which contains the *original* complex load circuit parameters (B_L, J_a, and B_a), can be accurately extracted. The loading effect, which reflects on the prior circuit parameters (J_{S1}, B_1, and J_{1L}), can also be extracted but will not be used.

Using the EM simulated S_{11} at one of the two ad-hoc ports in Fig. 5 with the other port terminated by a matched load, the rational function of the normalized input admittance Y_{in}, in terms of the lowpass domain complex frequency s, can be derived through vector fitting method [31] once the phase loading is removed [32]. The circuit parameters in Fig. 6 can be deduced from the rational function of admittance Y_{in} as follows:

The input admittance Y_{in} can be expressed as

$$Y_{\text{in}} = \frac{J_{S1}^2}{s + jB_1 + \frac{J_{1L}^2}{s+jB_L+\frac{J_a^2}{s+jB_a}}} \tag{3}$$

from which the input coupling inverter J_{S1} can be extracted by

$$J_{S1}^2 = sY_{\text{in}}|_{s\to\infty} \tag{4}$$

According to the definition of an admittance inverter

$$Y_1 = \frac{J_{S1}^2}{Y_{\text{in}}} = s + jB_1 + \frac{J_{1L}^2}{s + jB_L + \frac{J_a^2}{s+jB_a}} \tag{5}$$

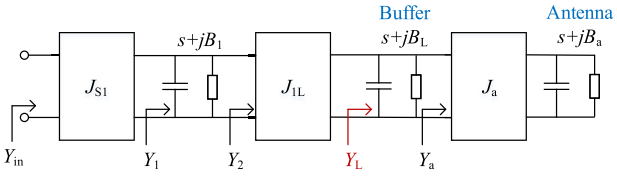

Fig. 6. Circuit model in the lowpass domain for the three-pole ALF for extraction of complex load.

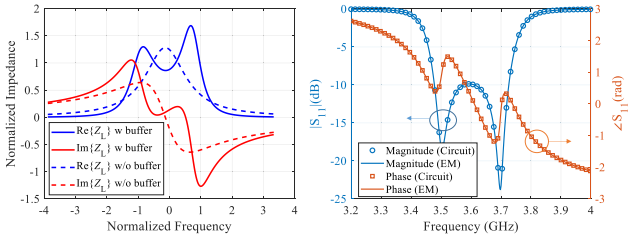

(a) (b)

Fig. 7. (a) Real and imaginary parts of complex impedance Z_L. (b) S_{11} of the EM simulated and circuit model of the three-pole MDR patch ALF.

from which B_1 can be obtained by

$$jB_1 = (Y_1 - s)|_{s\to\infty} \tag{6}$$

Consequently

$$Y_2 = Y_1 - s - jB_1 = \frac{J_{1L}^2}{s + jB_L + \frac{J_a^2}{s+jB_a}} \tag{7}$$

The same process is repeated until the remaining parameters J_{1L}, B_L, J_a, and B_a are extracted. It is worth mentioning that in obtaining the EM simulated S_{11}, the two ad-hoc ports in the EM model must exhibit sufficiently high isolation so that the extracted complex load will not be affected by the other polarization signal path.

By applying the extraction procedure described by (3) through (7), the circuit parameters of the complex load are obtained as follows: $B_L = 0.057 - j0.0385$, $J_a = 0.9304 - j0.0207$, $B_a = 0.1317 - j0.7804$. The resonant frequencies and losses of resonators are clearly reflected in their respective extracted circuit parameters. As expected, the patch antenna can be regarded as a high-loss resonator with a resonant frequency slightly lower than the center frequency of the filter. Having obtained the complex FIR of the antenna B_a, The equivalent unloaded Q of the antenna can be calculated to be 19.76 using

$$Q = \frac{f_0}{\text{BW}} \cdot \frac{1}{|\text{Im}\{B_a\}|} \tag{8}$$

With the circuit model in Fig. 6 obtained, the complex load impedance Z_L can be determined by

$$Z_L = \frac{1}{Y_L} = \frac{1}{s + jB_L + \frac{J_a^2}{s+jB_a}} \tag{9}$$

whose frequency characteristics along with those of the antenna without the buffer are superimposed in Fig. 7(a). It is evidenced that the buffer resonator introduces an additional peak for the real part and two more turning points for the imaginary part of the complex load within the passband of

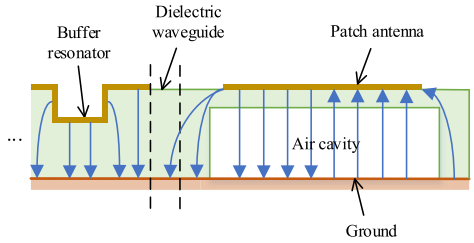

Fig. 8. Electric field lines along the central line in the vicinity of the dielectric waveguide.

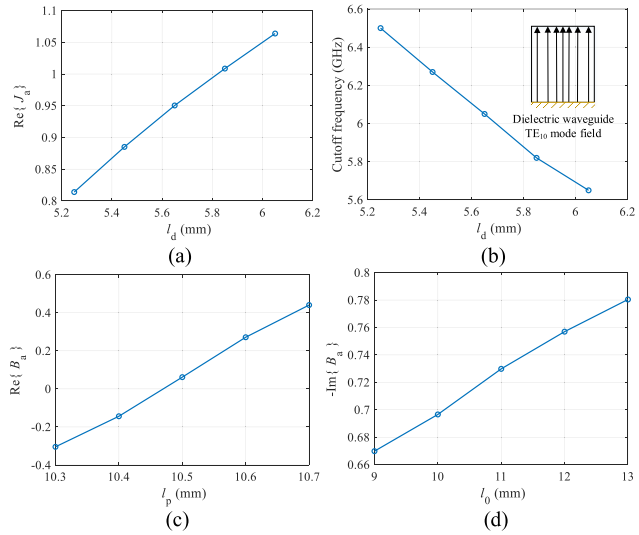

Fig. 9. (a) $\mathrm{Re}\{J_a\}$ versus l_d. (b) Cutoff frequency of dielectric waveguide versus l_d. (c) $\mathrm{Re}\{B_a\}$ versus l_p. (d) $-\mathrm{Im}\{B_a\}$ versus l_0.

the filter, making the complex impedance flatter comparatively. Excellent agreement on S_{11} between the EM simulation and extracted model can be observed in Fig. 7(b), justifying the circuit model in Fig. 6.

C. Analysis of Antenna and Its Feeding Dielectric Waveguide

To feed the patch antenna without significantly perturbing its current due to the metalized surface of the monoblock filter pair, a short evanescent-mode dielectric waveguide is employed as the coupling element between the buffer resonator (in quasi-TEM mode) and the substrate-based patch antenna (in TM_{01} mode) in a monoblock manner. In other words, the admittance inverter J_a is implemented using the dielectric waveguide. The electric field lines along the central line in the vicinity of the waveguide and patch antenna are depicted in Fig. 8, showing their compatibility with the electric fields of the buffer resonator.

The value of the admittance inverter J_a is primarily affected by the waveguide width l_d, height h, and length t. For compactness and compatibility of the structure, the waveguide height and length are fixed at $h = 6$ mm and $t = 1.5$ mm, respectively, but its width l_d can be adjusted. Fig. 9 illustrates how these critical dimensions affect the inverter J_a, the frequency offset of the antenna $\mathrm{Re}\{B_a\}$, and the radiation conductance of the antenna -$\mathrm{Im}\{B_a\}$. As shown in Fig. 9(a) and (b), $\mathrm{Re}\{J_a\}$ increases, and the cutoff frequency

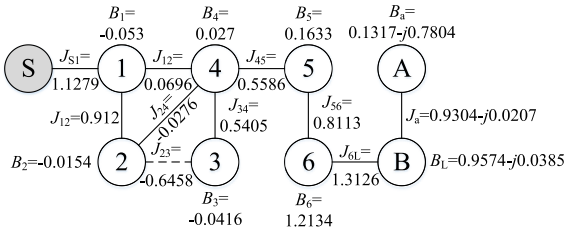

Fig. 10. Topology of the ALF with synthesized coupling coefficients. (B: buffer. A: antenna).

TABLE III
SYNTHESIZED COEFFICIENTS OF REALIZABLE POLYNOMIALS

$s^i, i =$	$E''(s)$	$F''(s)$	$P''(s)$
0	0.3399+j0.0776	0.0204+j0.0212	j5.0066
1	1.3787+j0.3400	0.0697+j0.1322	-0.3042
2	2.8927+j0.7018	0.4046+j0.3992	j1
3	3.8650+j0.9334	0.3039+j0.6106	
4	3.7114+j0.6999	1.2905+j0.5471	
5	2.2237+j0.4371	0.3208+j0.4371	
6	1	1	
	$\varepsilon'' = 14.413$, $\theta = 0.733$ rad		

of the TE_{10}-like mode in the waveguide decreases as the width l_d increases, resembling an inductive coupling window between two waveguide resonators. Fig. 9(c) demonstrates that the self-coupling of the antenna $\mathrm{Re}\{B_a\}$ increases as the patch size l_p increases, indicating a decrease in the resonant frequency. A significant phenomenon is presented in Fig. 9(d), which reveals that the equivalent radiation conductance of the antenna $-\mathrm{Im}\{B_a\}$ increases as l_0 increases. This observation aligns with the understanding that a patch antenna with a lower dielectric constant has a broader bandwidth.

D. Synthesis of the Bandpass Filter

With the circuit model of the antenna and the buffer resonator extracted in the presence of the monoblock filter body, the 6-2 coupled-resonator filter can be synthesized to achieve a required return loss of 18 dB in the frequency band of 3.5–3.72 GHz. The chosen coupling topology of the filter is presented in Fig. 10, where "B" and "A" represent the buffer resonator and antenna, respectively. Two designated TZs at 3.35 and 3.85 GHz, essentially for fulfilling the rejection specification, are realized by a CQ section.

Applying the theory of filter synthesis with a frequency-variant complex load, an antenna-loaded 6-2 filter is synthesized with the extracted complex load Z_L. Fig. 11(a) and (b) show the responses of the synthesized realizable filter with the complex load and a unity reference load, respectively. The synthesized polynomials $[E''(s), P''(s), F''(s)]$ and the electrical length θ of the inserted TL are listed in Table III. Using the synthesized $[E''(s), P''(s), F''(s)]$, θ, and transformation in (2), the overall circuit parameters can be directed obtained, including the relevant ones in Fig. 3: $B'_N = 1.2134$, $J'_{NL} = 1.3126$, and $B_0 = 0.9$. The designated topology with synthesized circuit parameters of the overall network is shown in Fig. 10, where the FIR jB_0 has been absorbed into the original self-coupling of the buffer

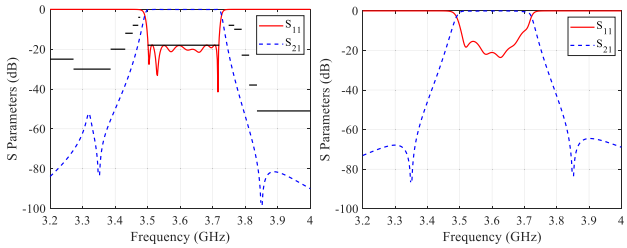

Fig. 11. Synthesized response of the ALF with design specs for port impedance of (a) complex load and (b) unity real load.

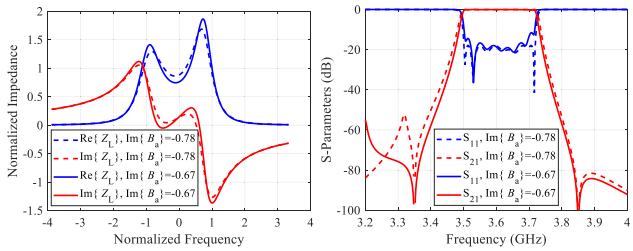

Fig. 12. (a) Real and imaginary parts of complex impedance and (b) synthesized responses with $\mathrm{Im}\{B_a\} = -0.78$ and -0.67.

resonator, presenting an eight-pole coupled-resonator network. Due to the relatively large value of θ, the self-couplings of resonator 6 and the buffer resonator, after absorbing the FIR, are relatively large, resulting in a resonance in the lower stopband, as seen in Fig. 11(a). Fortunately, the spike of the unwanted resonance in the rejection response is at the level of -50 dB, significantly lower than the specification. It can be confirmed that the out-of-band resonance does not contribute noticeably to the in-band insertion loss and the rejection rate of the ALF.

E. Dominance of Antenna Radiation Conductance

The radiation conductance determines the matching bandwidth of an antenna. In the context of the circuit model of the ALF shown in Figs. 6 and 10, the conductance (normalized) is represented by the imaginary part of B_a. As discussed in Section III-C, a larger negative $\mathrm{Im}\{B_a\}$ corresponds to a lower antenna Q factor and a wider antenna bandwidth. The normalized complex load impedances and the synthesized filter responses for $\mathrm{Im}\{B_a\} = -0.78$ and -0.67 are compared in Fig. 12, which correspond to the air cavity dimensions of $l_0 = 13$ and 9 mm, respectively. It is seen that a larger negative value of $\mathrm{Im}\{B_a\}$ results in flatter complex impedance characteristics, thus a wider matching bandwidth. To create a large radiation conductance in the physical design of the monoblock ALF module, carving out an air cavity in the ceramic substrate underneath the patch antenna from the bottom is a critical means.

Considering the overall ALF configuration and the thickness of the supporting substrate, the antenna bandwidth has been maximized with the best effort. The radiation conductance $1/R = |\mathrm{Im}\{B_a\}|$ in this example is approximately 0.78. In the traditional synthesis of a filtering antenna, the antenna Q factor is required to be equal to the filter external Q factor, or equivalently, $1/R = J_{NL}^2 Z_0$, where $Z_0 = 1$ and J_{NL} is the output coupling of a traditional filter terminated by real loads. If the traditional synthesis approach was used with the same specifications, the objective radiation conductance $J_{NL}^2 Z_0 \approx 0.92$ would be too large to be achieved by the antenna in this example.

F. Role of Antenna in Frequency Selectivity

While an antenna can be modeled by a resonator in an ALF, as verified above, the frequency selectivity of the antenna will not be as good as that of a dedicated resonator. This point has never been clearly discussed in the existing literature, leading to various misunderstandings. To clarify this point, Fig. 13 compares S_{21} (dB) for three scenarios with the same return loss and TZs: 1) a regular 7-2 filter (seventh-order filter with two TZs); 2) a 6-2 filter loaded with a buffer resonator and an antenna (eight poles in total); and 3) a regular 8-2 filter. The regular filters are synthesized using traditional filter synthesis theory. To ensure a fair comparison in the stopband, the eight-pole ALF is synthesized without any out-of-band resonance. The same B_a but different B_L and J_a are used in the complex load. It can be observed that the out-of-band rejection rate of the eight-pole ALF falls between those of the regular 7-2 and 8-2 filters but is closer to that of the 7-2 filter. This observation indicates that the antenna contributes to certain rejection characteristics but is only equivalent to a half-order resonator at most.

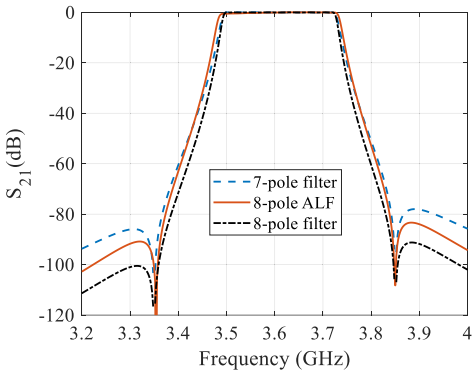

Fig. 13. Comparison of S_{21}(dB) of an ALF with regular filters.

IV. Deterministic EM Design of the Monoblock ALF

After synthesizing the ALF network, the next step is to design the physical model of the monoblock dual-polarized ALF pair deterministically. The design philosophy involves extracting the overall circuit model using a novel technique called the VIP model and identifying the directions for dimensional adjustments. The adjustment is based on the differences between the synthesized circuit model and the extracted model in an EM "tuning" stage.

A. VIP Port for Model Extraction of ALF

Given that an ALF is a single-terminal passive network, the return loss S_{11} alone is insufficient to obtain a complete

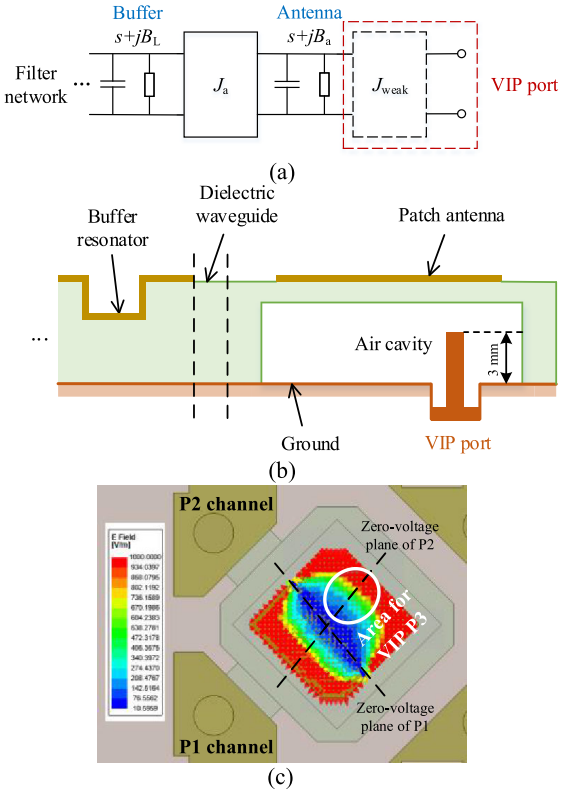

Fig. 14. (a) Circuit model of VIP port. (b) Cross section of antenna with VIP port. (c) Electric field distribution underneath the metal patch with P1 excited.

circuit model, not to mention the rejection characteristic. To overcome this limitation, a VIP port is introduced at the antenna end, as depicted in Fig. 14(a). A VIP port must fulfill two requirements: 1) the I/O coupling of the port must be sufficiently weak to minimize the perturbation of the antenna field and the return loss of the concerned polarization and 2) the signal from the VIP port must not interfere with the other polarization path for a dual-polarized ALF.

To fulfill requirement 1, the VIP port is required to provide an appropriate weak coupling. As a rule of thumb, the transmission coefficient of the signal path should be approximately −20 dB. The VIP port in this example is realized by a coaxial probe with the inner conductor suspended in the air under the patch antenna, as illustrated in Fig. 14(b). It is found that a 3 mm probe can provide a reasonable transmission level. To satisfy requirement 2, the probe of the VIP port is positioned at a null-field spot of the electric field when the port of the other polarization is excited. Fig. 14(c) illustrates the electric field of the metal patch when P1 is excited, displaying the field pattern of the TM_{01} mode. To pair with P1, the VIP P3 is slightly offset from the zero-voltage plane for P1 to achieve a weak I/O coupling but aligns with the zero-voltage plane for P2. The final position of the VIP port corresponding to P1 is (−2.8, 0.3) mm relative to the center of the antenna substrate.

To verify the position of the VIP port, the extracted circuit parameters of the three-pole model in Fig. 5 with and without the VIP port are found to differ by less than 0.01, which is sufficiently small. The in-band transmission coefficient between P3 and P2 is approximately −30 dB, which is sufficiently weak to prevent any interference from the P3 signal path.

TABLE IV
DIFFERENCES BETWEEN EXTRACTED AND SYNTHESIZED REAL PARTS OF CIRCUIT PARAMETERS OF THE ALF

Circuit Parameter	Stage 1	Stage 2	Stage 3	Stage 4	Final
J_{S1}	**-0.0411**	-0.0156	0.0046	0.0043	0.0018
J_{12}	-0.003	0.0031	0.0036	0.006	0.0063
J_{14}	-0.0039	-0.0005	-0.002	-0.0009	-0.0035
J_{23}	**0.0324**	**0.0468**	-0.0056	-0.0003	0.0061
J_{24}	0.0096	0.0033	-0.0033	0.0002	-0.0035
J_{34}	-0.0135	**-0.0278**	**-0.0231**	0.0065	-0.0043
J_{45}	-0.003	-0.0054	-0.0034	-0.0012	0.0026
J_{56}	**0.0316**	0.0119	0.0248	0.0135	-0.0124
J_{6L}	**-0.0971**	-0.0032	**-0.0218**	-0.0086	0
J_a	**0.066**	**0.0352**	**0.0217**	**0.0266**	-0.0044
B_1	**-0.2281**	**-0.0984**	**0.0288**	-0.0061	-0.0035
B_2	**-0.0779**	**-0.0674**	0.0063	0.0042	0.0047
B_3	**-0.1944**	**-0.1098**	**-0.0403**	-0.0049	0.0015
B_4	**-0.0942**	**-0.0352**	**-0.0375**	-0.001	0.001
B_5	**0.1139**	**0.0521**	**0.0746**	0.0099	-0.007
B_6	**0.0336**	**-0.0221**	**0.0431**	0.0115	-0.022
B_L	**-0.1397**	0.0183	-0.0312	-0.0207	0.0217
B_a	**-0.5743**	0.0172	**0.034**	0.0174	-0.0157

B. Overall Model Extraction and Deterministic EM Design

With the VIP port introduced, the EM-simulated S-parameters between P1 and P3 can be acquired. These parameters will be used to extract the overall circuit model, which has the same coupling topology as shown in Fig. 10, using model-based vector fitting (MVF) [33] as if for a regular two-port filter.

When designing one channel of the ALF in the presence of a three-port network, the other channel serves as a weakly coupled load. The design method for the six-pole filter with a buffer resonator is exactly the same as that for a regular coupled-resonator filter, provided that the overall circuit parameters can be extracted smoothly. With the extracted circuit model, not only can the coupled-resonator filter network be tuned accordingly, but also the antenna and the dielectric waveguide. The tuning direction is toward reducing the difference between the extracted and synthesized target circuit models. The EM tuning process from stage 1 to stage 4 is illustrated in Fig. 15, showing continuous improvement. The differences between the extracted and synthesized real parts of the circuit parameters (labeled in Fig. 10) of stages 1 through 4 and the final stage are listed in Table IV. The differences decrease as the EM tuning process goes on, showing the effectiveness of the deterministic EM design process. Note that the EM model is lossy, leading to negligible imaginary parts of the resonator circuit parameters in the extracted circuit model, which are not displayed in the table. Introducing the VIP port is the final touch in the proposed deterministic EM design process, enabling a highly efficient tuning process of the ALF module.

To illustrate the accuracy of the extracted circuit model, the final EM responses, along with those from the extracted circuit model, are plotted in Fig. 16(a)–(c), showing excellent

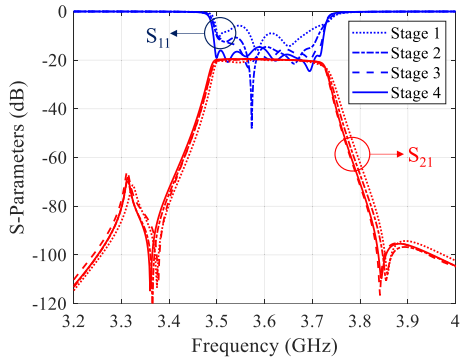

Fig. 15. Responses of EM tuning process from stage 1 to stage 4.

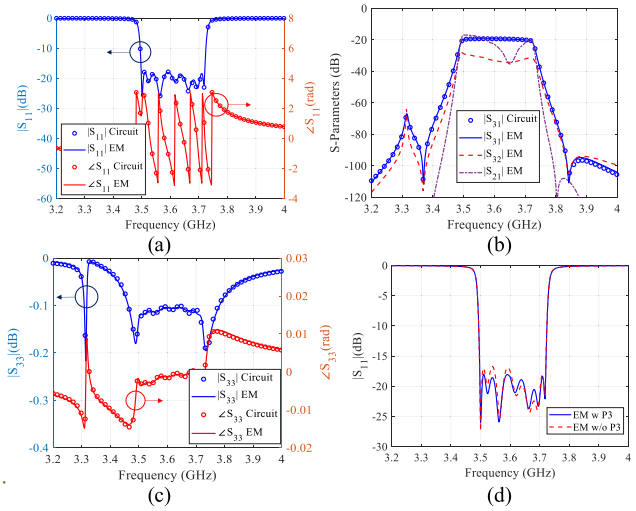

Fig. 16. (a) EM and extracted S_{11}. (b) EM and extracted S_{31}, EM S_{32}, and EM S_{21}. (c) EM and extracted S_{33}. (d) EM S_{11} with and without VIP P3.

agreement. Unlike a lossless filter network, there is a significant difference between the magnitude of S_{11} and S_{33} due to the high antenna radiation loss. The level of the S_{31} magnitude in the passband is around -20 dB, as expected, which is over 10 dB higher than that of S_{32}. The VIP P3 is highly mismatched, as evidenced by the reflection coefficient S_{33} being only around -0.1 dB. To accurately fit the very weak trans-admittance Y_{13} using MVF, the parameter w in the weighting factor $1/(|Y_{13}|)^w$ is set to around 0.62 in this example.

In EM simulation results, an input return loss of 18 dB is achieved as synthesized. The transmission response in the passband exhibits a high isolation of approximately 20 dB between the two polarization channels. The deep notch in the isolation in the passband is attributed to the cancellation of the originally coupled signal and an interference signal from the surroundings. Two prescribed TZs are realized around 3.35 and 3.85 GHz. The S_{11} (dB) with and without the virtual port P3 are compared in Fig. 16(d), showing little effect of the VIP port on the response.

The proposed synthesis and EM design framework of an ALF can be summarized in the following steps:

1) Choose physical realizations of the filter and antenna and construct a low-order EM model for extracting the circuit model of the antenna as the complex load in the presence of the filter body.
2) Synthesize the filter network with the extracted complex load while managing to increase the radiation conductance if necessary.
3) Add a VIP port at the antenna end with a weak coupling for extracting the overall circuit model from the EM simulation results of the ALF physical model.
4) Adjust the physical model by minimizing the difference between the extracted and synthesized ALF model until a satisfactory response is achieved, where the difference is sufficiently small.

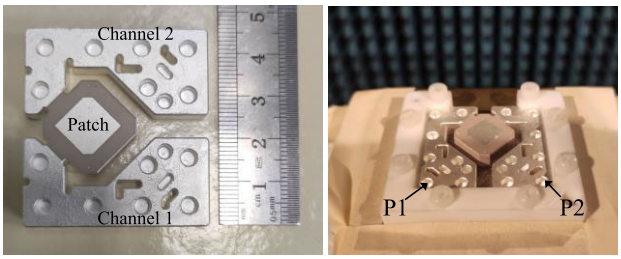

Fig. 17. Photograph of the fabricated monoblock dual-polarized ALF pair in (a) top view and (b) in the antenna measurement setup.

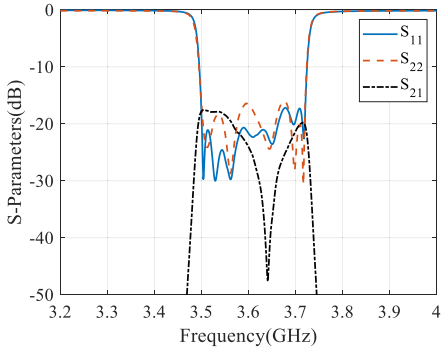

Fig. 18. Measured S-parameters of the prototype.

V. Measurement Results

To validate the concept of the monoblock ALF module and the synthesis and EM design framework, the EM-designed monoblock dual-polarized patch ALF module is fabricated and fine-tuned to achieve excellent filtering and radiation characteristics.

The fabricated prototype of the ALF module is displayed in Fig. 17. Due to inevitable manufacturing errors, post-fabrication fine-tuning is necessary to achieve satisfactory performance. During the tuning process, the resonant frequency of a resonator can be tuned by scraping the metal surface of its blind hole. The final measured S-parameters of ports 1 and 2 of the ALF module are presented in Fig. 18. The measured return loss of 16 dB for both polarizations and good isolation with the worst value of 17.5 dB in the working frequency band is achieved.

The EM simulated and measured realized gain and total efficiency versus frequency of ports P1 and P2 are compared in Fig. 19. The EM simulation results show two radiation nulls

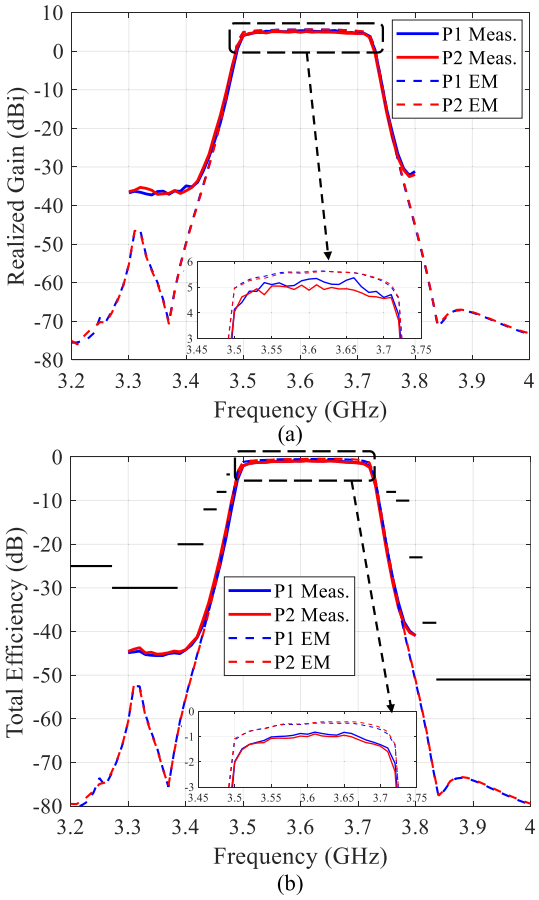

Fig. 19. EM simulated and measured (Meas.) (a) realized gains and (b) total efficiencies of ports P1 and P2.

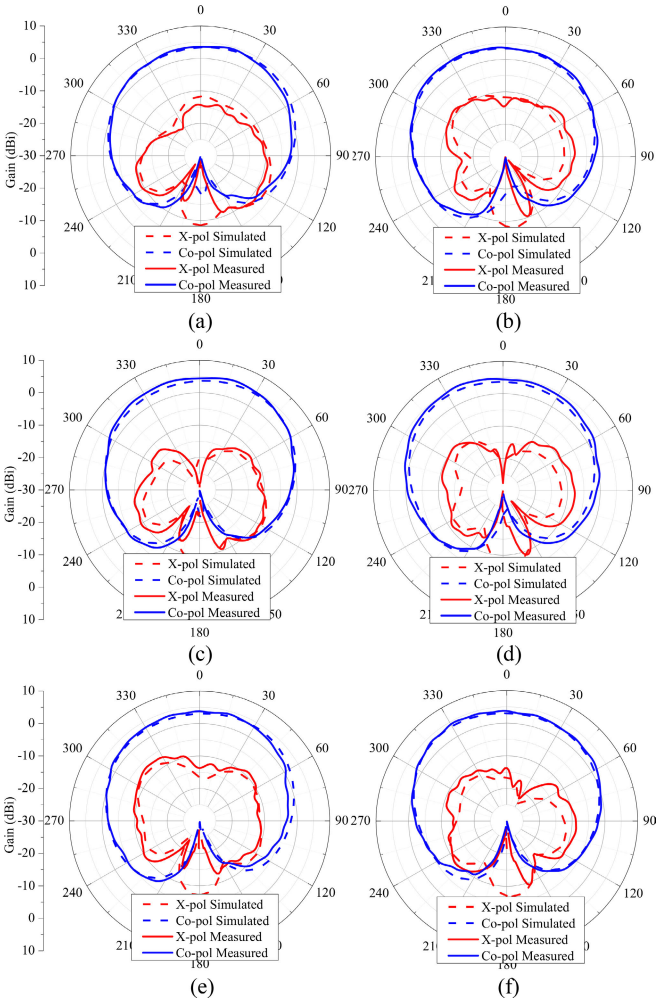

Fig. 20. EM simulated and measured radiation patterns when P1 is excited at (a) and (b) 3.5 GHz, (c) and (d) 3.61 GHz, and (e) and (f) 3.72 GHz in the plane of $\phi = 0°/90°$.

achieved by the two TZs of the filter network. These nulls enable a high rejection of 29 and 34 dB at 50 MHz from the lower and higher band edges, respectively. Due to the limited noise floor in the antenna gain measurement, the two nulls cannot be manifested in the measurement result. Nevertheless, a stable measured in-band gain of approximately 5.22 dBi is achieved, and the frequency selectivity agrees well with the EM simulated one. The measured total efficiency of the ALF module at 3.61 GHz is −0.86 dB or equivalently 82%. The majority of the loss is attributed to the filter insertion loss.

It is worth mentioning that for the purpose of comparison, the same monoblock ALF pair with a different set of coupling coefficients is also synthesized and EM designed, in which no out-of-band resonance is introduced. The comparison of the EM-simulated radiation efficiencies in the passband shows that the chosen design option with the buffer resonator and out-of-band resonance exhibits 0.1 dB less insertion loss.

The EM simulated and measured radiation patterns with port P1 excited at the center and edge frequencies are plotted in Fig. 20. The monoblock dual-polarized ALF module exhibits a significantly better symmetrical radiation pattern compared to the single-polarized ALF case [26], in which the symmetry of the structure is poor. Additionally, it exhibits a superior cross-polarization discrimination (XPD) level of 32.1 dB at boresight ($\theta = 0°$) and 12 dB at $\theta = \pm 60°$ at the center frequency. The excellent radiation characteristics are attributed to the balanced structure design of the monoblock ALF pair.

TABLE V
COMPARISON WITH OTHER FILTERING ANTENNAS

Ref.	Filter order	Unloaded Q	Polari-zation	FBW(%)	RL(dB)	Selectivity (dB/GHz)
[3]	4	Medium	Single	6.2	13	131
[4]	2	Medium	Single	3	6	45
[6]	3	Low	Single	12.5	14	68
[9]	4	Medium	Single	7.64	10	375
[10]	4	High	Single	6.43	15	136
[11]	1	Low	Single	2	12	213
[14]	2	Low	Dual	12.3	14	28
[16]	3	Low	Dual	13.1	13	189
[18]	N.A.		Single	20.3	10	68
[19]			Dual	8.2	15	100
[20]			Single	53.5	14	51
[21]			Single	9.14	10	213
This	**6**	**High**	**Dual**	**6.1**	**16**	**680**

FBW: Fractional bandwidth. RL: Return loss.

The performance of the proposed monoblock dual-polarized ALF pair is compared with other reference filtering antennas in Table V. To provide an intuitive comparison, the selectivity is examined, which is defined as (20–3 dB)/$|f_{20\text{ dB}} - f_{3\text{ dB}}|$, where $f_{20\text{ dB}}$ and $f_{3\text{ dB}}$ represent the frequencies in GHz at rejection levels of 20 and 3 dB, respectively. This metric essentially measures the roll-off rate of rejection levels

from 3 to 20 dB. The higher selectivity in the lower and upper stopband is selected. Notably, the presented monoblock ALF module achieves superior frequency selectivity over other works within a comparable volume. The frequency selectivity of the proposed scheme can be flexibly controlled by the filter order and TZ arrangement. Although a narrowband antenna is used in this work, the ALF model achieves a relatively high return loss level within the designated frequency band. The unloaded Q of the dielectric resonator in the monoblock ALF pair, referring to the data in [24], is the highest among all reported filtering antenna schemes.

VI. Conclusion

This article proposes a monoblock dual-polarized ALF pair, along with a comprehensive framework encompassing circuit model extraction, direct filter synthesis, and deterministic EM design. This is the first time to synthesize an ALF using the direct synthesis theory of a filter with a complex load. The synthesis theory offers two key advantages. First, the filter is synthesized by fully considering the optimally designed antenna as a frequency-variant complex load. Second, the synthesized circuit model serves as the EM design target due to its one-to-one correspondence to physical realization. This approach addresses the limitation of the traditional filtering antenna synthesis approach by increasing the design freedom, especially for narrowband antennas.

To extract the overall circuit model of an ALF module for EM tuning, the concept of a VIP model is proposed, in which a weakly coupled port at the antenna end is introduced. It enables the extraction of a complete circuit model of a physical ALF module heuristically, including the antenna element. It also allows for a deterministic and highly efficient EM tuning process. The proposed synthesis and EM design framework is generic and can be applied to other types of ALF modules.

To address the challenge of the narrow antenna bandwidth, an additional buffer resonator, prefixed to the patch antenna, is innovatively introduced. Having artistically created a symmetrical surrounding for the antenna element, the monoblock $\pm 45^\circ$ dual-polarized ALF pair exhibits high-frequency selectivity, excellent in-band matching, and superior radiation characteristics with a high total efficiency. It is anticipated that the proposed framework will be widely used in the design of various ALF modules and that the design practice will serve as a valuable case study for the industry.

References

[1] T. E. Nadan, J. P. Coupez, S. Toutain, and C. Person, "Integration of an antenna/filter device, using a multi-layer, multi-technology process," in *Proc. 28th Eur. Microw. Conf.*, Oct. 1998, pp. 672–677.

[2] H. Blondeaux et al., "Radiant microwave filter for telecommunications using high Qu dielectric resonator," in *Proc. 30th Eur. Microw. Conf.*, Oct. 2000, pp. 1–4.

[3] Y. Yusuf and X. Gong, "Compact low-loss integration of high-Q 3-D filters with highly efficient antennas," *IEEE Trans. Microw. Theory Techn.*, vol. 59, no. 4, pp. 857–865, Apr. 2011.

[4] Y. Yusuf, H. Cheng, and X. Gong, "A seamless integration of 3-D vertical filters with highly efficient slot antennas," *IEEE Trans. Antennas Propag.*, vol. 59, no. 11, pp. 4016–4022, Nov. 2011.

[5] W.-J. Wu, Y.-Z. Yin, S.-L. Zuo, Z.-Y. Zhang, and J.-J. Xie, "A new compact filter-antenna for modern wireless communication systems," *IEEE Antennas Wireless Propag. Lett.*, vol. 10, pp. 1131–1134, 2011.

[6] Z. H. Jiang and D. H. Werner, "A compact, wideband circularly polarized co-designed filtering antenna and its application for wearable devices with low SAR," *IEEE Trans. Antennas Propag.*, vol. 63, no. 9, pp. 3808–3818, Sep. 2015.

[7] C.-X. Mao et al., "An integrated filtering antenna array with high selectivity and harmonics suppression," *IEEE Trans. Microw. Theory Techn.*, vol. 64, no. 6, pp. 1798–1805, Jun. 2016.

[8] R. H. Mahmud and M. J. Lancaster, "High-gain and wide-bandwidth filtering planar antenna array-based solely on resonators," *IEEE Trans. Antennas Propag.*, vol. 65, no. 5, pp. 2367–2375, May 2017.

[9] H.-Y. Xie, B. Wu, Y.-L. Wang, C. Fan, J.-Z. Chen, and T. Su, "Wideband SIW filtering antenna with controllable radiation nulls using dual-mode cavities," *IEEE Antennas Wireless Propag. Lett.*, vol. 20, no. 9, pp. 1799–1803, Sep. 2021.

[10] J. Rao, K. Nai, P. Vaitukaitis, Y. Li, and J. Hong, "3-D metal printed compact high-Q folded waveguide filter with folded antenna," *IEEE Trans. Microw. Theory Techn.*, vol. 70, no. 1, pp. 112–121, Jan. 2022.

[11] C.-K. Lin and S.-J. Chung, "A compact filtering microstrip antenna with quasi-elliptic broadside antenna gain response," *IEEE Antennas Wireless Propag. Lett.*, vol. 10, pp. 381–384, 2011.

[12] L.-H. Wen et al., "A balanced feed filtering antenna with novel coupling structure for low-sidelobe radar applications," *IEEE Access*, vol. 6, pp. 77169–77178, 2018.

[13] Y. Xu, L. Zhu, and N.-W. Liu, "Differentially fed wideband filtering slot antenna with endfire radiation under multi-resonant modes," *IEEE Trans. Antennas Propag.*, vol. 67, no. 10, pp. 6650–6655, Oct. 2019.

[14] Y. Li, Z. Zhao, Z. Tang, and Y. Yin, "Differentially fed, dual-band dual-polarized filtering antenna with high selectivity for 5G sub-6 GHz base station applications," *IEEE Trans. Antennas Propag.*, vol. 68, no. 4, pp. 3231–3236, Apr. 2020.

[15] C. Fan, B. Wu, Y.-L. Wang, H.-Y. Xie, and T. Su, "High-gain SIW filtering antenna with low H-plane cross polarization and controllable radiation nulls," *IEEE Trans. Antennas Propag.*, vol. 69, no. 4, pp. 2336–2340, Apr. 2021.

[16] K.-R. Xiang, F.-C. Chen, Q. Tan, and Q.-X. Chu, "High-selectivity filtering patch antennas based on multipath coupling structures," *IEEE Trans. Microw. Theory Techn.*, vol. 69, no. 4, pp. 2201–2210, Apr. 2021.

[17] X. Y. Zhang, W. Duan, and Y. M. Pan, "High-gain filtering patch antenna without extra circuit," *IEEE Trans. Antennas Propag.*, vol. 63, no. 12, pp. 5883–5888, Dec. 2015.

[18] P. F. Hu, Y. M. Pan, X. Y. Zhang, and S. Y. Zheng, "A compact filtering dielectric resonator antenna with wide bandwidth and high gain," *IEEE Trans. Antennas Propag.*, vol. 64, no. 8, pp. 3645–3651, Aug. 2016.

[19] W. Duan, X. Y. Zhang, Y. M. Pan, J. X. Xu, and Q. Xue, "Dual-polarized filtering antenna with high selectivity and low cross polarization," *IEEE Trans. Antennas Propag.*, vol. 64, no. 10, pp. 4188–4196, Oct. 2016.

[20] Z. Wei, Z. Zhou, Z. Tang, J. Y. Yin, J. Ren, and Y. Yin, "Broadband filtering magnetoelectronic dipole antenna with quasi-elliptic gain response," *IEEE Trans. Antennas Propag.*, vol. 68, no. 4, pp. 3225–3230, Apr. 2020.

[21] Q. Liu and L. Zhu, "A compact wideband filtering antenna on slots-loaded square patch radiator under triple resonant modes," *IEEE Trans. Antennas Propag.*, vol. 70, no. 10, pp. 9882–9887, Oct. 2022.

[22] B. Yuan, "Filter and transceiver comprising dielectric body resonators having frequency adjusting holes and negative coupling holes," U.S. Patent 9 998 163 B2, Jun. 12, 2018.

[23] Y. Chen, Y. Zhang, and K.-L. Wu, "A dual-mode monoblock dielectric bandpass filter using dissimilar fundamental modes," *IEEE Trans. Microw. Theory Techn.*, vol. 69, no. 8, pp. 3811–3819, Aug. 2021.

[24] Y. Zhang, Y. Chen, and K. Wu, "A dispersive quadruplet structure for monoblock dielectric resonator filters," *IEEE Trans. Microw. Theory Techn.*, vol. 70, no. 6, pp. 3105–3114, Jun. 2022.

[25] Y. Zhang, F. Seyfert, and K.-L. Wu, "Dispersive box section and its applications to quasi-TEM mode monoblock dielectric filters," *IEEE Trans. Microw. Theory Techn.*, vol. 71, no. 3, pp. 1136–1147, Mar. 2023.

[26] X. Tan, Y. Chen, and K.-L. Wu, "A monoblock dielectric resonator filtering patch antenna," in *Proc. 17th Eur. Conf. Antennas Propag. (EuCAP)*, Florence, Italy, Mar. 2023, pp. 1–4.

[27] H. Meng and K.-L. Wu, "Direct optimal synthesis of a microwave bandpass filter with general loading effect," *IEEE Trans. Microw. Theory Techn.*, vol. 61, no. 7, pp. 2566–2573, Jul. 2013.

[28] K. Kurokawa, "Power waves and the scattering matrix," *IEEE Trans. Microw. Theory Techn.*, vol. MTT-13, no. 3, pp. 194–202, Mar. 1965.
[29] K.-L. Wu and W. Meng, "A direct synthesis approach for microwave filters with a complex load and its application to direct diplexer design," *IEEE Trans. Microw. Theory Techn.*, vol. 55, no. 5, pp. 1010–1017, May 2007.
[30] P. Zhao and K.-L. Wu, "An iterative and analytical approach to optimal synthesis of a multiplexer with a star-junction," *IEEE Trans. Microw. Theory Techn.*, vol. 62, no. 12, pp. 3362–3369, Dec. 2014.
[31] H. Hu and K.-L. Wu, "A generalized coupling matrix extraction technique for bandpass filters with uneven-Qs," *IEEE Trans. Microw. Theory Techn.*, vol. 62, no. 2, pp. 244–251, Feb. 2014.
[32] M. Meng and K.-L. Wu, "An analytical approach to computer-aided diagnosis and tuning of lossy microwave coupled resonator filters," *IEEE Trans. Microw. Theory Techn.*, vol. 57, no. 12, pp. 3188–3195, Dec. 2009.
[33] P. Zhao and K.-L. Wu, "Model-based vector-fitting method for circuit model extraction of coupled-resonator diplexers," *IEEE Trans. Microw. Theory Techn.*, vol. 64, no. 6, pp. 1787–1797, Jun. 2016.

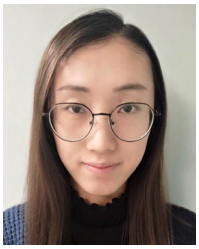

Xiao Tan received the B.Eng. and Ph.D. degrees from The Chinese University of Hong Kong, Hong Kong, in 2018 and 2024, respectively, both in electronic engineering.

Her current research interests include complex-loaded filter synthesis, filtering antennas, and MIMO antenna arrays for BS applications.

Yuliang Chen (Member, IEEE) received the B.Eng. degree in electromagnetic field and wireless technology from Northwestern Polytechnical University, Xi'an, China, in 2017, and the Ph.D. degree in electronic engineering from The Chinese University of Hong Kong, Hong Kong SAR, in 2024.

His current research interests include miniaturization techniques and robot automatic tuning of microwave filtering components for wireless communications.

Dr. Chen was a recipient of the Best Paper Award of the 2020 IEEE (HK) AP/MTT Postgraduate Conference.

Ke-Li Wu (Fellow, IEEE) received the B.S. and M.Eng. degrees from Nanjing University of Science and Technology, Nanjing, China, in 1982 and 1985, respectively, and the Ph.D. degree from Laval University, Quebec, QC, Canada, in 1989.

From 1989 to 1993, he was a Research Engineer at McMaster University, Hamilton, ON, Canada. He joined COM DEV (now Honeywell Aerospace), Cambridge, ON, Canada, in 1993, where he was a Principal Member of Technical Staff. Since 1999, he has been with The Chinese University of Hong Kong, Hong Kong, where he is currently a Professor and the Director of the Radio Frequency Radiation Research Laboratory. His current research interests include EM-based circuit domain modeling of high-speed interconnections, robot automatic tuning of microwave filters, decoupling techniques of MIMO antennas, and IoT technologies.

Prof. Wu is a member of the IEEE MTT-5 Technical Committee. He was a recipient of the 1998 COM DEV Achievement Award and the Asia–Pacific Microwave Conference Prize twice in 2008 and 2012, respectively. He was an Associate Editor of IEEE TRANSACTIONS ON MICROWAVE THEORY AND TECHNIQUES from 2006 to 2009.